Chaotic Modeling and Simulation (CMSIM) 2: 323-335, 2012

A Sub Microscopic Description of the Formation of Crop Circles

Volodymyr Krasnoholovets[1] and Ivan Gandzha[2]

Indra Scientific, Square de Solbosch 26, Brussels, B-1050, Brussels, Belgium
(E-mail: [1] v_kras@yahoo.com, [2] gandzha@iop.kiev.ua)

Abstract: We describe a sub microscopic mechanism that is responsible for the appearance of crop circles on the surface of the Earth. It is shown that the inner reason for the mechanism is associated with intra-terrestrial processes occurring in the outer core and the mantle of the terrestrial globe. We assume that magnetostriction phenomena should take place at the boundary between the liquid and the solid nickel-iron layers of the terrestrial globe. Our previous studies showed that at the magnetostriction a flow of inertons takes out of the striction material (inertons are carriers of the field of inertia, they represent a substructure of the matter waves, or the particle's psi-wave function; they transfer mass properties of elementary particles and are able to influence massive objects changing their inner state and behaviour). At the macroscopic striction in the interior of the Earth, pulses of inerton fields are irradiated, and through non-homogeneous channels of the globe's mantle and crust they reach the surface of the Earth. Due to the interaction with walls of these channels, fronts of inerton flows come to the surface as fringe images. These inerton flows affect local plants and bend them, which results in the formation of the so-called crop circles. It is argued that the appearance of crop circles under the radiation of inertons has something in common with the mechanism of formation of images in a kaleidoscope, which happens under the illumination of photons.
Keywords: Crop circles, Inertons, Mantle and Crustle channels, Magnetostriction of rocks.

1 Introduction

Crop circles attract attention of many researchers. Studies (see, e.g. Refs. 1-3) show that in these circles stalks are bent up to ninety degrees without being broken and something softened the plant tissue at the moment of flattening. Something stretches stalks from the inside; sometimes this effect is so powerful that the node looks as exploded from the inside out. In many places crop formation is accompanied with a high degree of magnetic susceptibility, which is caused by adherent coatings of stalks with the commingled iron oxides, hematite (Fe_20_3) and magnetite (Fe_30_4) fused into a heterogeneous mass [2].
Researchers [2-4] hypothesized that crop formations involve organised ion plasma vortices, which deliver lower atmosphere energy components of

Received: 18 July 2011 / Accepted 30 March 2012

ISSN 2241-0503

sufficient magnitude to produce bending of stalks, the formation of expulsion cavities in plant stems and significant changes in seedling development.
It should be noted that an idea of the origin of crop circles associated with the atmosphere energy and/or UFO is generally accepted.
On the other hand, researchers who study geophysical processes and the earthquakes note about possible regional semi-global magnetic fields that might be generated by vortex-like cells of thermal-magmatic energy, rising and falling in the earth's mantle [5]. Another important factor is magnetostriction of the crust – the alteration of the direction of magnetization of rocks by directed stress [6,7].
Moreover, recent study [8] has suggested a possible mechanism of earthquake triggering due to magnetostriction of rocks in the crust. The phenomenon of magnetostriction in geophysics is stipulated by mechanical deformations of magnetic minerals accompanied by changes of their remanent or induced magnetization. These deformations are specified by magnetostriction constants, which are proportional coefficients between magnetization changes and mechanical deformations. A real value of the magnetostriction constant of the crust is estimated as about 10^{-5} ppm/nT, which is a little larger than for pure iron. Yamazaki's calculation [8] shows that effects connected to the magnetostriction of rocks in the crust can produce forces nearly 100 Pa/year and even these comparatively small stress changes can trigger earthquakes.
Of course, weaker deformations associated with magnetostriction of rocks also take place. These are the magnetostriction deformations that we put in the foundation of the present study of field circles.

2 Preliminaries

Our theoretical and experimental studies have shown that the phenomenon of magnetostriction is accompanied with the emission of inerton fields from the magnetostrictive material studied. What is the inerton field?
Bounias and one of the authors [9-12] proposed a detailed mathematical theory of the constitution of the real physical space. In line with this theory, real space is constrained to be a mathematical lattice of closely packed topological balls with approximately the Planck size, $\sqrt{\hbar G/c^3} \approx 10^{-35}$ m. It was proven that such a lattice is a fractal lattice and that it also manifests tessellation properties. It has been called a tessel-lattice. In the tessel-lattice volumetric fractalities of cells are associated with the physical concept of mass. A particle represents a volumetrically deformed cell of the tessel-lattice. The motion of such a particle generates elementary excitations of the tessel-lattice around the particle. These excitations, which move as a cloud around the particle, represent the particle's force of inertia. That is why they were called inertons [13,14]. The corresponding submicroscopic mechanics developed in the real space can easily be connected to conventional orthodox quantum mechanics constructed in an abstract phase space. Submicroscopic mechanics associates the particle's cloud of inertons with the quantum mechanical wave ψ-function of this particle. Thus,

the developing concept turns back a physical sense to the wave ψ-function: this function represents the field of inertia of the particle under consideration. Carriers of the field of inertia are inertons. A free inerton, which is released from the particle's cloud of inertons, possesses a velocity that exceeds the velocity of light [15].

In condensed media entities vibrating at the equilibrium positions periodically irradiate and absorb their clouds of inertons back [16]; owing to such a behaviour the mass of entities varies. This means that under special conditions the matter may irradiate a portion of its inertons. Lost inertons then can be absorbed by the other system, which has to result in changes of physical properties of the system.

One of such experiments was carried out in work [17]. Continuous-wave laser illumination of ferroelectric crystal of $LiNbO_3$ resulted in the production of a long-living stable electron droplet with a size of about 100 μm, which freely moved with a velocity of about 0.5 cm/s in the air near the surface of the crystal experiencing the Earth's gravitational field. The role of the restraining force of electrons in the droplet was attributed to the inerton field, a substructure of the particles' matter waves, which was expelled from the surface of crystal of $LiNbO_3$ together with photoelectrons by a laser beam. Properties of electrons after absorption of inertons changed very remarkably – they became heavy electrons whose mass at least million of times exceeded the rest mass of free electrons. Only those heavy electrons could elastically withstand their Coulomb repulsion associated with the electrical charge, which, of course, is impossible in the case of free electrons.

We have shown [16] that in the chemical industry inerton fields are able to play the role of a field catalyst or, in other words, inerton fields can serve to control the speed of chemical reactions. In the reactive chamber we generated inerton fields by using magnetostriction agents: owing to the striction the agents non-adiabatically contract, which is culminated in the irradiation of sub matter, i.e. inertons, from the agents. Then under the inerton radiation, the formation of a new chemical occurred in several seconds, though usually these chemical reactions last hours.

Therefore, these results allow us to involve inerton fields, which originate from the ground, in a study of the formation of crop circles.

The thickness of the crust is about 20 km. The mantle extends to a depth above 3000 km. The mantle is made of a thick solid rocky substance. Due to dynamical processes in the interior of the Earth, magnetostrictive rocks contract with a coefficient of about 10^{-5} [8], which is a trigger mechanism for the appearance of a flow of inerton radiation. This flow of inertons shoots up from a depth by coming through the mantle and crust channel. Such channels are usual terrestrial materials with some non-homogenous inclusions down to tens or hundreds of kilometers from the surface of the terrestrial globe (compare with bio-energy channels in our body: the crude morphological structure is the same, but the fine morphological structure is different, which allows these bio-energy channels to display a higher conductivity).

A mantle-crust channel can be modeled as a cylindrical tube, which has a cross-section area equal to A, along which a flow of inertons travels out from the interior of the globe. The inner surface of the channel has to reflect inerton radiation, at least partly, so that the flow of inertons will continue to follow along the channel to its output, i.e. the surface of the Earth.

3 Elastic rod bending model

Let us evaluate conditions under which the stalks of herbaceous plants will bend affected by mantle insertions.

A stalk of a plant can be modeled for the first approximation by an elastic rod (Fig. 1). We suppose that it is deformed by an external force distributed uniformly over the rod length. This external force is a force caused by a flow of inertons going from the ground due to a weak collision of the mantle and crust rocks as described above. The rod profile in the projections to the horizontal and vertical axes is described as follows [18].

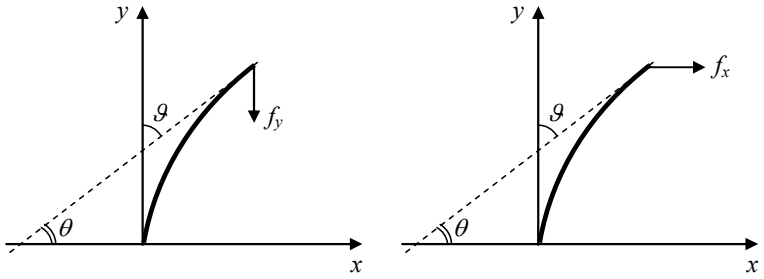

Fig. 1. Elastic rod model.

I. Vertical force f_y (Fig. 1a)

$$x=\sqrt{\frac{2IE}{f_y}}\left(\sqrt{1-\cos\vartheta_l}-\sqrt{\cos\vartheta-\cos\vartheta_l}\right),\quad y=\sqrt{\frac{IE}{2f_y}}\int_0^{\vartheta}\frac{\cos\vartheta\,d\vartheta}{\sqrt{\cos\vartheta-\cos\vartheta_l}}. \quad (1)$$

Here $I=\pi R^4/4$ is the rod's moment of inertia, R is the rod's radius, and E is the Young's modulus of the rod's material. The length of the rod is explicitly given as

$$l=\sqrt{\frac{IE}{2f_y}}\int_0^{\vartheta}\frac{d\vartheta}{\sqrt{\cos\vartheta-\cos\vartheta_l}}. \quad (2)$$

At the maximum bending we have $\vartheta_{\max}=\vartheta_l=\pi/2$, so that

$$l=\sqrt{\frac{IE}{2f_y}}\int_0^{\pi/2}\frac{d\vartheta}{\sqrt{\cos\vartheta}}=\sqrt{\frac{IE}{f_y}}\,K(1/2), \quad (3)$$

where $K(1/2)\approx 1.854$ is the complete elliptic integral of the first kind. Hence, we come to an expression for the force required to bend the rod by a $\pi/2$ angle:

$$f_y = \frac{IE}{l^2} K^2(1/2) \approx 3.44 \frac{IE}{l^2}. \quad (4)$$

II. Horizontal force f_x (Fig. 1b)

$$x = \sqrt{\frac{IE}{2f_x}} \int_0^{\vartheta} \frac{\sin \vartheta d\vartheta}{\sqrt{\sin \vartheta_l - \sin \vartheta}}, \qquad y = \sqrt{\frac{2IE}{f_x}} \left(\sqrt{\sin \vartheta_l} - \sqrt{\sin \vartheta_l - \sin \vartheta} \right) \quad (5)$$

The length of the rod is explicitly given as

$$l = \sqrt{\frac{IE}{2f_x}} \int_0^{\vartheta} \frac{d\vartheta}{\sqrt{\sin \vartheta_l - \sin \vartheta}}. \quad (6)$$

In this case the maximum bending angle should be smaller than $\pi/2$ (no such a force exists that can bend the rod by this angle). So, we select the maximum bending angle at $\vartheta_l = \pi/3$ and write the corresponding relationship between the rod's length and the acting force:

$$l \approx \sqrt{\frac{IE}{2f_x}}\, 2.61 \quad \text{or} \quad f_x \approx 3.41 \frac{IE}{l^2}, \quad (7)$$

which is nearly the same as in the previous case (4).

Now let us evaluate the value of the breaking force $f_{break} = f_x \cong f_y$. We have to substitute numerical values $l = 0.5$ m, $R = 1.5 \times 10^{-3}$ m for the rod and the value of elasticity (Young's) modulus E to expressions (4) or (7). The value of E has been measured for many different grasses, see, e.g., Refs. 19-23. According to these data, E varies approximately from (0.8 to about 1)$\times 10^9$ kg/(m·s^2). For instance, in the case of wheat we can take $E \approx 3 \times 10^9$ kg/(m·s^2), which gives for the horizontal breaking force (7)

$$f_{\text{break}} = f_x \approx 3.41 \frac{IE_{\text{Young}}}{l^2} \approx 0.163 \text{ N}. \quad (8)$$

Besides, the authors [19-23] emphasize that for grassy stalks in addition to the elasticity modulus one has to take into account the bending stress, the yield strength (tensile strength) and the shearing stress. These parameters range from 7×10^6 to about 50×10^6 kg/(m·s^2) and, hence, significantly decrease the real value of f, which is capable to bend stalks. For example, putting for E the value of the maximal tensile stress 50×10^6 kg/(m·s^2) we obtain for the bending non-breaking force

$$f_{\text{bend}} = f_x \approx 3.41 \frac{IE_{\text{tens}}}{l^2} \approx 0.0027 \text{ N}. \quad (9)$$

The gravity force acting on the rod is

$$f_{\text{grav}} = mg = \rho V g = \pi \rho R^2 l g \approx 0.033 \text{ N}. \quad (10)$$

where ρ is the rod's material density about $\rho = 10^3$ kg/m^3, m and V are its mass and volume, and $g = 9.8$ m/s^2 is the acceleration due to gravity.

Thus we may conclude that any extraneous force F applied to a grassy stalk will be able to fold the stalk to the ground if the value of the force satisfies inequalities

$$f_{\text{bend}} \le F \le f_{\text{break}} \quad (11)$$

4 Motion of the rotating central field

The inner surface of a mantle-crust channel can be described by a retaining potential U, which is holding a flow of inertons spreading along the channel from an underground source. Let μ be the mass of an effective batch of terrestrian inertons from this source, which interact with a grassy stalk. The planar motion of such a batch of inertons in the central field is described by the Lagrangian

$$L = \frac{\mu}{2}\left(\dot{r}^2 + r^2\dot{\varphi}^2\right) - U(r,\dot{\varphi}) \tag{12}$$

which is here written in polar coordinates r and φ; dot standing for the derivative with respect to time. To model a spreading inerton field, the potential should include a dependence on the angular velocity, $U(r, \dot{\varphi})$, which means that we involve the proper rotation of the Earth relative to the flow of inertons. For instance, the potential can be chosen in the form of the sum of two potentials:

$$U(r,\dot{\varphi}) = \frac{\alpha}{2}r^2 + \frac{\beta}{2}r^2\dot{\varphi}\,. \tag{13}$$

In the right hand side of expression (12) the first term is a typical central-force harmonic potential, which describes an elastic behaviour of the batch of inertons in the channel and the surrounding space; the second term includes a dependence on the azimuthal velocity, which means that it depicts the rotation-field potential. The introduction of this potential allows us to simulate more correctly the reflection of inertons from the walls of the mantle channel, which of course only conditionally can be considered round in cross-section.
The equations of motion are then written as

$$\frac{d}{dt}\frac{\partial L}{\partial \dot{q}_i} - \frac{\partial L}{\partial q_i} = 0\,, \quad i = 1,\ 2, \quad q_1 \equiv \rho, \quad q_2 \equiv \varphi \tag{14}$$

or in the explicit form

$$\ddot{r} - r\dot{\varphi}^2 + \frac{\alpha}{\mu}r + \frac{\beta}{\mu}r\dot{\varphi} = 0\,, \tag{15}$$

$$r\ddot{\varphi} + 2\dot{r}\cdot\left(\dot{\varphi} - \frac{\beta}{2\mu}\right) = 0\,. \tag{16}$$

These equations can be integrated explicitly or solved numerically at the given initial conditions $r(0)$, $\dot{r}(0)$, $\varphi(0)$, $\dot{\varphi}(0)$, and the trajectory of motion can be plotted in rectangular coordinates $\{r\cos\varphi,\ r\sin\varphi\}$. The second equation represents the conservation of the angular momentum M:

$$\frac{d}{dt}\left[\mu r^2\cdot\left(\dot{\varphi} - \frac{\beta}{2\mu}\right)\right] = 0 \quad \text{or} \quad M = \mu r^2\cdot\left(\dot{\varphi} - \frac{\beta}{2\mu}\right) = \text{const}\,. \tag{17}$$

Figures 2 and 5 show two possible trajectories at particular values of the parameters. The radius of the inner circle is governed by the parameter β/μ.

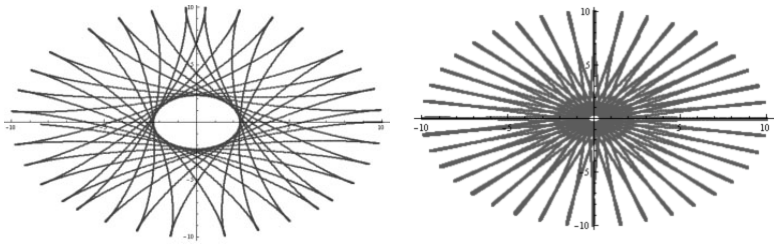

Fig. 2. Trajectories of the motion of inertons in the rotating central field. Parameters for the left figure: $\alpha/\mu = 1$ s^{-2}, $\beta/\mu = 0.5$ s^{-1}; $r(0) = 10$ m, $\dot{r}(0) = 0$, $\varphi(0) = 0$, $\dot{\varphi}(0) = 0.01$ s^{-1}. Parameters of the right figure: $\alpha/\mu = 1$ s^{-2}, $\beta/\mu = 0.1$ s^{-1}; $r(0) = 10$ m, $\dot{r}(0) = 0$, $\varphi(0) = 0$, $\dot{\varphi}(0) = 0.01$ s^{-1}.

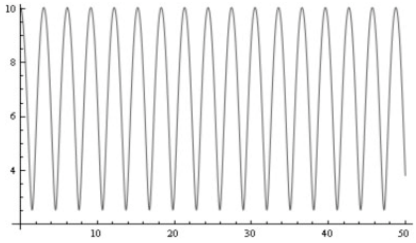

Fig. 3. Velocity $|\dot{\vec{r}}| = \sqrt{\dot{r}^2 + r^2\dot{\varphi}^2}$ of the batch of inertons versus time for the case of the trajectory shown in Fig. 2 (left). The max. velocity is $\upsilon_{\max} = 10$ m/s.

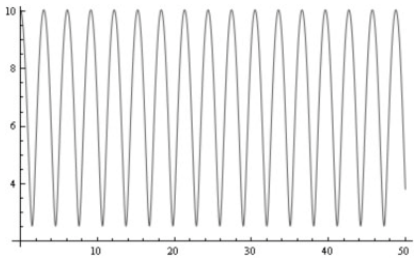

Fig, 4. Acceleration $|\ddot{\vec{r}}| = \sqrt{(\ddot{r} - r\dot{\varphi}^2)^2 + (2\dot{r}\dot{\varphi} + r\ddot{\varphi})^2}$ of the batch of inertons versus time for the case of the trajectory shown in Fig. 2 (left). The maximal acceleration is $a_{\max} \approx 10$ m/s^2.

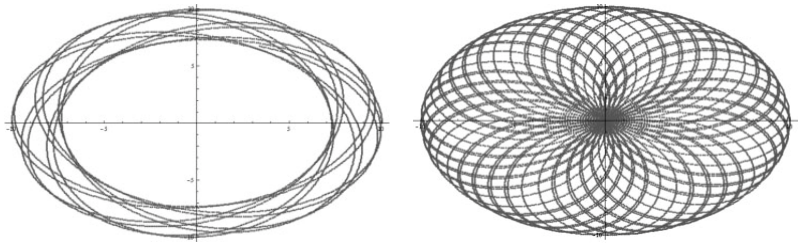

Fig. 5. Trajectory of the motion of inertons in the rotating central field. Parameters for the right figure: $\alpha/\mu = 1$ s^{-2}, $\beta/\mu = 0.5$ s^{-1}; $r(0) = 10$ m, $\dot{r}(0) = 0$, $\varphi(0) = 0$, $\dot{\varphi}(0) = 1$ s^{-1}. Parameters for the left figure: $\alpha/\mu = 1$ s^{-2}, $\beta/\mu = 2$ s^{-1}; $r(0) = 10$ m, $\dot{r}(0) = 0$, $\varphi(0) = 0$, $\dot{\varphi}(0) = 1$ s^{-1}.

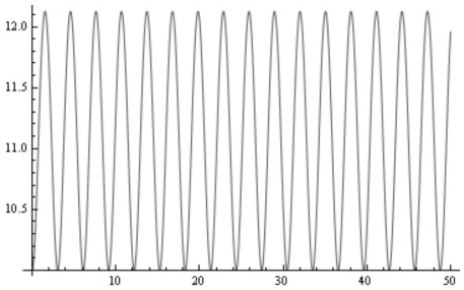

Fig. 6. Velocity $|\dot{\vec{r}}| = \sqrt{\dot{r}^2 + r^2\dot{\varphi}^2}$ of the batch of inertons versus time for the case of the trajectory shown in Fig. 5 (left). The max. velocity is $\upsilon_{\max} \approx 12$ m/s.

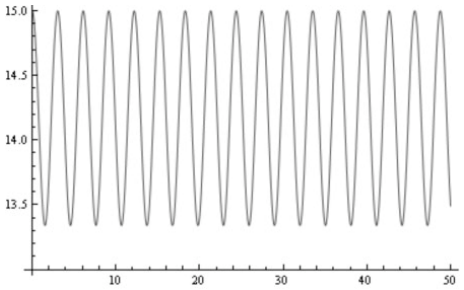

Fig. 7. Acceleration $|\ddot{\vec{r}}| = \sqrt{(\ddot{r} - r\dot{\varphi}^2)^2 + (2\dot{r}\dot{\varphi} + r\ddot{\varphi})^2}$ of the batch of inertons
versus time for the case of the trajectory shown in Fig. 5 (left). The maximal acceleration is $a_{\max} \approx 15$ m/s^2.

In the case of the Newton-type potential, expression (13) changes to

$$U(r,\dot{\varphi}) = -\frac{\gamma}{r} + \frac{\beta}{2} r^2 \dot{\varphi}. \tag{18}$$

Then the equations of motion for the Lagrangian (14) become

$$\ddot{r} - r\dot{\varphi}^2 + \frac{\gamma}{\mu r^2} + \frac{\beta}{\mu} r\dot{\varphi} = 0, \tag{19}$$

$$\ddot{r} - r\dot{\varphi}^2 + \frac{\gamma}{\mu r^2} + \frac{\beta}{\mu} r\dot{\varphi} = 0. \tag{20}$$

the solution to these equations is shown in Fig. 8.

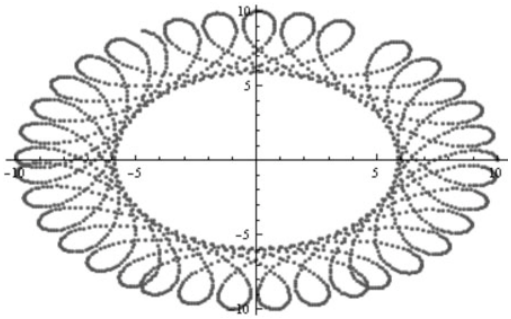

Fig. 8. Trajectory of the motion of inertons in the rotating central field with parameters $\gamma/\mu = 1$ m^3 s^{-2}, $\beta/\mu = 0.1$ s^{-1}; $r(0) = 10$ m, $\dot{r}(0) = 0$, $\varphi(0) = 0$, $\dot{\varphi}(0) = 0.01$ s^{-1}.

In Fig. 9 we show the solution to the equations of motion of a batch of inertons for the case of simplified potential (18), namely, when it is represented only by the Newton-type potential $U(r) = -\gamma/r$.

Figures 4 to 7 give an estimate for the acceleration a of the batch of inertons: $a = 10$ to 15 m/s^2.

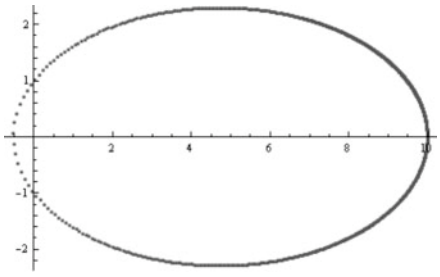

Fig. 9. Elliptic trajectory of the motion of inertons in the Newton-type potential with parameters $\gamma/\mu = 1$ m^3·s^{-2}, $\beta/\mu = 0$ s^{-1}; $r(0) = 10$ m, $\dot{r}(0) = 0$, $\varphi(0) = 0$, $\dot{\varphi}(0) = 0.01$ s^{-1}.

Figures 2, 4, 8 and 9 depict possible patterns of crop circles generated by flows of the mantle-crust inertons.

Let us estimate now the intensity of inerton radiation needed to form a crop circle of total area $A \approx 100$ m^2. Let M_{rocks} be the mass of the mantle-crust rocks that generate inertons owing to their magnetostriction activity. We have to take into account the magnetostriction coefficient C, which describes an extension strain of rocks. In view of the fact of that low frequencies should accompany geophysical dynamical processes, we can assume that the striction activity of a local group of rocks occurs at a low frequency ν (i.e. rocks collide N times per a time Δt of radiation of inertons). Having these parameters, we can evaluate a flow of mass μ_Σ that is shot in the form of inerton radiation at the striction of rocks: $\mu_\Sigma \approx N C M_{\text{rocks}}$.

If we put $M \sim 10^7$ kg, $C \sim 10^{-5}$, and $N = 5$ we obtain $\mu_\Sigma \approx 500$ kg. This mass μ_Σ is distributed along the area of A in the form of a flow of the inerton field. Let each square metre be the ground for the growth of 1000 stalks. Then 10^5 stalks can grow in the area of $A = 100$ m^2. This means that each stalk is able to catch an additional mass $\mu = \mu_\Sigma / 10^5 = 5$ g from the underground inerton flow; this value is of the order of the mass of a stalk itself.

Knowing the mass $\mu = 5 \times 10^{-3}$ kg of the batch of inertons which interacts with a stalk and the acceleration of this inerton batch $a = 10$ to 15 m/s^2, we can rate the force of inertons that bends and breaks up stalks in the large area A: $F = \mu a \approx 0.05$ to 0.075 N. This estimation exceeds not only the threshold bending force f_{bend} (9), but also the gravity force f_{grav} (10). At the same time the inerton force F does not break physically the stalk, because the value of F still satisfies inequalities (11). Therefore, the model developed in this work is plausible.

A flow of mass, which is coming as a pulse of inertons from the interior of the Earth to its surface, partly compensates the gravitational acceleration at the Earth surface $g = GM_{\text{Earth}} / R^2_{\text{Earth}} = 9.81\,\text{m}\cdot\text{s}^{-1}$. This statement can be verified in places where crop circles appear most frequently.

5 Kaleidoscope model

This kaleidoscope model gives a static description of inerton structures. We assume that a bunch of inertons depicted in the centre of Fig. 10 is reflected from the walls, whose geometry was selected rectangular in this particular example. Multiple reflections from the walls produce the pattern shown in Fig. 10. This model can be assumed as an analogy of geometrical optics with light reflecting from the mirrors. Uniting the rotating central field model described in the previous section and the kaleidoscope model can generate yet more complex patterns.

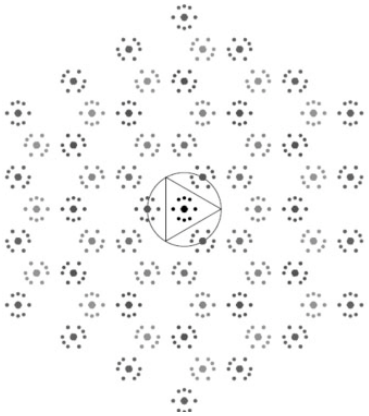

Fig. 10. Kaleidoscope mode

6 Conclusions

In this study we have shown a radically new approach to the conception and description of crop circles. The theory developed is multi-aspect and based on first submicroscopic principles of fundamental physics. The theory sheds light also on fine processes occurring in the crust and the mantle of the terrestrial globe.
The investigation will allow following researchers to improve the mathematical model of the description of shapes of crop circles, to correctly concentrate on biological changes in plants taken from crop circles, to reach more progress in understanding a subtle dynamics of the earth crust, and to contemplate a more delicate approach to the development of new methods of earthquake prediction.

Acknowledge

The authors thank greatly Prof. Christos H. Skiadas for the invitation to take part in the 4th Chaotic Modelling and Simulation International Conference (CHAOS 2011, Agio Nicolaos, Crete, May-June 2011) at which this work was presented.

References

1. W. C. Levengood. Anatomical anomalies in crop formation plants, *Physiologia Plantarum* 92**:**356-363, 1994.

2. W. C. Levengood and J. Bruke. Semi-Molten Meteoric Iron Associated with a Crop Formation, *J. Scient. Exploration* 9:191-199, 1995. C. H. Skiadas. Two simple models for the early and middle stage prediction of innovation diffusion. *IEEE Trans Eng Manage* 34:79–84, 1987.

3. J. A. Bruke. The physics of crop formations, *MUFON Journal*, October, 3-7, 1998.

4. W. C. Levengood and N. P. Talbott, Dispersion of energies in worldwide crop formations, *Physiologia Plantarum* 105:615-624, 1999. A sigmoid stochastic growth model derived from the revised exponential. In: Janssen J, Skiadas CH (eds) *Applied Stochastic Models and Data Analysis*. World Scientific, Singapore, pp 864–870, 1993.

5. J.-C. Pratsch. Reative motion in geology: some philosophical differences, *J. Petroleum Geology* 13:229–234, 1990.

6. W. H. Munk and G. J. F. Macdonald. *The Rotation of the Earth. A Geophysical Discussion*, Cambridge University Press, London, 1975.

7. H. Jeffreys. *The earth. Its origin, history and physical constitution*, Cambridge University Press, London, 1976.

8. K. Yamazaki. Possible mechanism of earthquake triggering due to magnetostriction of rocks in the crust, *American Geophysical Union, Fall Meeting 2007*, abstract #S33B-1307, Dec. 2007.

9. M. Bounias and V. Krasnoholovets. Scanning the structure of ill-known spaces: Part 1. Founding principles about mathematical constitution of space, *Kybernetes: The Int. J. Systems and Cybernetics* 32:945-975, 2003; arXiv.org: physics/0211096.

10. M. Bounias and V. Krasnoholovets. Scanning the structure of ill-known spaces: Part 2. Principles of construction of physical space, *ibid*. 32:976-1004, 2003; arXiv: physics/0212004.

11. M. Bounias and V. Krasnoholovets. Scanning the structure of ill-known spaces: Part 3. Distribution of topological structures at elementary and cosmic scales, *ibid*. 32:1005-1020, 2003; arXiv: physics/0301049.

12. M. Bounias and V. Krasnoholovets. The universe from nothing: A mathematical lattice of empty sets. *Int. J. Anticipatory Computing Systems* 16:3-24, 2004; arXiv.org: physics/0309102.

13. V. Krasnoholovets. Submicroscopic deterministic quantum mechanics, *Int. J. Computing Anticipatory Systems* 11:164-179, 2002; arXiv: quant-ph/0109012.

14. V. Krasnoholovets. Inerton fields: Very new ideas on fundamental physics, *American Inst. Phys. Conf. Proc.* – Dec. 22, 2010 – Volume 1316, 244-268. Search for fundamental theory: The VII International Symposium Honouring French Mathematical Physicist Jean-Pierre Vigier (12-14 July 2010, Imperial College, London); doi:10.1063/1.3536437.

15. V. Krasnoholovets and J.-L. Tane. An extended interpretation of the thermodynamic theory including an additional energy associated with a decrease in mass, *Int. J. Simulation and Process Modelling* 2:67-79, 2006; also arXiv.org: physics/0605094.

16. V. Krasnoholovets. Variation in mass of entities in condensed media, *Applied Physics Research* 2:46-59, 2010.

17. V. Krasnoholovets, N. Kukhtarev and T. Kukhtareva. Heavy electrons: Electron droplets generated by photogalvanic and pyroelectric effects. *Int. J. Modern Phys. B* 20:2323-2337, 2006; arXiv.org: 0911.2361[quant-ph].

18. L. D. Landau and E. M. Lifshits, *The theory of elasticity*, Nauka, Moscow, 1987, pp. 106-107 (in Russian).
19. G. Skubisz. The dependence of the Young's modulus of winter wheat stalk in various phenological phases, *Proceedings of the 2nd International Conference on physical properties of agricultural materials*, Godollo, Hungary, 26-28 August 1980, Vol. 2., 1980, p. 9.
20. G. H. Dunn and S. M. Dabney. Modulus of elasticity and moment of inertia of grass hedge stems, *Transactions of the ASAE* 39:947-952, 1996.
21. M. Nazari Galedar, A. Jafari, S. S. Mohtasebi, A. Tabatabaeefar, A. Sharifi, M. J. O'Dogherty, S. Rafiee and G. Richard. Effects of moisture content and level in the crop on the engineering properties of alfalfa stems, *Biosystems Engineering* 101: 199-208, 2008.
22. H. Tavakoli, S.S. Mohtasebi and A. Jafari. Effects of moisture content, internode position and loading rate on the bending characteristics of barley straw, *Research in Agricultural Engineering* 55:45-51, 2009.
23. A. Esehaghbeygi, B. Hoseinzadeh, M. Khazaei and A. Masoumi, Bending and shearing properties of wheat stem of alvand variety, *World Applied Sciences J*. 6:28-1032, 2009.

.